Chinese Chemical Letters 35 (2024) 108351

Contents lists available at ScienceDirect

Chinese Chemical Letters

journal homepage: www.elsevier.com/locate/cclet

Strategies to accelerate bubble detachment for efficient hydrogen evolution

Weinan Yin[a], Lexing Yuan[a], Hao Huang[a], Yuntao Cai[a], Junan Pan[a], Ning Sun[a], Qiyu Zhang[a], Qianhe Shu[a], Chen Gu[a], Zechao Zhuang[b], Longlu Wang[a,*]

[a] College of Electronic and Optical Engineering & College of Flexible Electronics (Future Technology), Nanjing University of Posts & Telecommunications (NJUPT), Nanjing 210023, China
[b] Department of Chemistry, Tsinghua University, Beijing 100084, China

ARTICLE INFO

Article history:
Received 5 February 2023
Revised 15 February 2023
Accepted 16 March 2023
Available online 20 March 2023

Keywords:
Bubble effect
Electrocatalytic water splitting
Electrode design
External field
System upgrade

ABSTRACT

In the process of electrocatalytic water splitting, the management of gaseous products is an important task. Timely detachment of gaseous products from the electrode surface and the electrolyte is beneficial to the reduction of energy consumption of the electrolytic cell. In the existing industrial electrolytic cells, the circulating pump drives the electrolyte flowing to discharge the gaseous products. Up to now, several much more advanced strategies have been explored to deal with the negative effects of bubbles. In this review, we summarized various strategies for bubble detachment, including electrode design, external field imposing and system upgrading. We also elaborated the principle, functional features, practicability, advantages and limitations of each method. Finally, challenges and perspectives are also provided for the further development of advanced bubbles detachment strategies for efficient hydrogen evolution.

1. Introduction

Ever-growing energy demand companied with the emerging decarbonization in the global energy system make exploring sustainable clean energies high on the agenda. Hydrogen, especially green hydrogen, is regarded as a critical energy carrier which is possibly alternative to conventional fossil fuels in decarbonizing industry and society for its superb energy density and sustainable production [1–4]. Electrocatalytic water splitting is a simple but efficient method to convert renewable energy sources into green hydrogen [5–8]. Although numerous efforts have been taken to develop a variety of highly active electrocatalysts [9–14], most of these electrocatalysts' performance of the hydrogen evolution reaction (HER) were evaluated under the laboratory condition, which cannot sufficiently prove its feasibility for industrial-scale application.

In general, the total overpotential in the electrocatalytic water splitting is mainly determined by activation overpotential, Ohmic overpotential and concentration overpotential [15]. A large number of researchers focus on the design of highly active HER electrocatalysts with low activation overpotential [16–20], whereas Ohmic overpotential and concentration overpotential are often neglected. Ohmic overpotential and concentration overpotential are greatly influenced by bubble behaviors in the process of the HER [21,22], which is the main challenge of electrocatalytic water splitting, especially under the industrial high current density [23–25]. Therefore, it is essential to accelerate the bubble detachment for efficient hydrogen evolution. Till now, various strategies for bubble detachment have been developed, mainly from the perspective of electrode design [26–31], external field imposing [32–43] and system upgrade [44–49]. In terms of electrode design, the application of porous and integrated-structured electrode can effectively reduce the adhesion force between the bubble and the electrode surface, boosting the detachment of bubbles [50–54]. Besides, on the basis of the porous electrode, timely detachment of bubbles can also be achieved by making the electrolyte flow through a pump [49]. The bubble detachment could also be effectively promoted by imposing acoustic field [33,34,39,42], magnetic field [36–38,40,41], supergravity field [35,43,55,56], *etc.* In essence, imposing external fields is to break the equilibrium state of the bubble and accelerate the detachment of bubbles *via* the input of extra energy. Furthermore, upgrading the conventional electrocatalytic water splitting device is also an effective way to tackle the negative effect of bubbles. For example, converting a system with a three-phase interface to a system with a two-phase interface is a typical strategy of system upgrade [46,48]. Moreover, instead of detaching from the electrolyte, the transmission path of generated bubbles can be changed by a specific electrode so that bubbles can be directly col-

* Corresponding author.
E-mail address: wanglonglu@njupt.edu.cn (L. Wang).

https://doi.org/10.1016/j.cclet.2023.108351
1001-8417/

lected [44], which also provides a novel perspective for upgrading the system.

Herein, with regard to the effect of generated bubbles to electrocatalytic water splitting, especially under industrial high current density, we systematically summarize different sorts of strategies to mitigate the negative effects of bubbles and accelerate bubble detachment, including electrode design, external field and system upgrading. In addition, the principle, functional features, practicability, advantages and limitations of each method are also elaborated. Ultimately, we put forward an outlook for the further development of advanced bubbles detachment strategies for efficient hydrogen evolution. It is expected that this review can boost further research on bubble detachment from more diverse perspectives.

2. Negative effect of bubble

There is no denying the fact that generated gas bubbles in electrocatalytic water splitting do harm to the reaction itself [57–63]. First and foremost (Fig. 1A), bubbles which nucleate and grow on the surface of the catalyst can lead to an inactive area, separating electrolyte from the active sites [64]. If there is a strong adhesion force between the catalyst and the single bubble, it is consequently easier for catalysts to peel off from the substrates. Therefore, the shielding effect of bubbles could deactivate the catalyst and break its stability, making an increase in Ohmic overpotential meanwhile [65–71]. It was worth noting that simulation of the influence of different bubble sizes and quantities on the electrolyte potential distributions for 3D-printed Ni (3DP Ni), 3DP Ni sample obtained at 1100 °C (3DP Ni-1100), and nickel foam (NF) was carried out by Xu *et al.* [72] through COMSOL in Fig. 1B. It was found that the variation of local electrolyte potential can be barely neglected when the size of bubbles is much small. However, local electrolyte potential dramatically fluctuates with the increase of the bubble size, inducing a continuous concentration gradient between the electrolyte and electrode surface and contributing to the increase of concentration overpotential. Although the catalyst is exactly the same, there usually exists a big difference in the Tafel slope due to the effect of bubbles. Van der Heijden *et al.* [73] tried to eliminate the non-kinetic effect by controlling the rotation rate, using oxygen evolution reaction (OER) as a model reaction and $Ni_{80}Fe_{20}OOH$ as catalyst (Fig. 1C). It can be clearly observed that the Tafel slope turns to be stable with the increase of rotation rate, indicating that high rotation rate can overcome the non-kinetic effects induced by bubbles (Fig. 1D). In the practical industrial electrolytic cells, the circulating pump drives the electrolyte flowing to discharge the gaseous products [74–76]. Up to now, several much more advanced strategies have been explored to deal with the negative effects of bubbles.

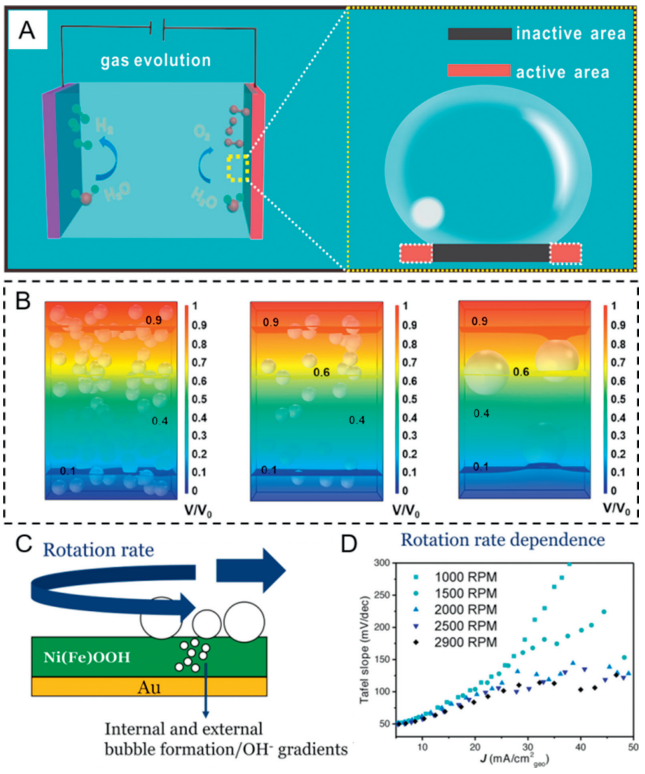

Fig. 1. (A) Schematic illustration of the growth of gas bubbles on a flat film electrode, which caused a large number of inactive sites to form. Reprinted with permission [64]. Copyright 2019, American Chemical Society. (B) Simulation of the influence of different bubble sizes and quantities on the electrolyte potential distributions for 3D-printed Ni (3DP Ni), 3DP Ni sample obtained at 1100 °C (3DP Ni-1100), and nickel foam (NF). Reprinted with permission [72]. Copyright 2023, American Chemical Society. (C) Schematic illustration of studying NiFeOOH catalysts for the alkaline oxygen evolution reaction (OER) with varying rotation rate. (D) Tafel slope *vs.* average current density (Tafel slope obtained over a 20 mV interval) under different rotation rate. Reprinted with permission [73]. Copyright 2022, Wiley VCH.

3. Electrode design

Generally, the generated gas bubbles start to nucleate on the surface of the electrode at first and keep growing before detaching in the process of electrocatalytic water splitting [77–84]. With the increase in the size of bubbles, the buoyancy force they suffer keeps growing accordingly until the buoyancy force overcomes the adhesion force which is exerted by the electrode [85,86]. As a common but effective strategy, the electrode or the catalyst is specifically designed to accelerate the detachment of bubbles, among which imparting superaerophobicity to the electrode is widely used [87–92]. Besides, both the size and the behavior of bubbles can also be changed to realize fast bubble detachment by means of electrode design [64,93].

3.1. Gradient porous electrode inducing bubble detachment

An efficient strategy to enhance the HER activity is to design new electrodes with superior porous structures where bubbles can be rapidly emitted from the electrode surface [94–100]. Recently, Yang *et al.* [101] have demonstrated that the gradient porous electrode (SML-LMS-HE) with decreasing apertures from the middle to the sides exhibited excellent HER activity with an overpotential of 83 mV at $-10\ mA/cm^2$ and appreciable durability. This electrode structure inducing bubble splitting to expose more active sites has great application prospects in the field of hydrogen production.

By simply pressing nickel foams with different porosities and loading MoS_2/Ni_3S_2 heteronanorods on their surface by solvothermal treatment (Fig. 2A), two types of gradient porous electrode with a decreasing pore size (SML-LMS) and an increasing pore size (LMS-SML) from the middle to the sides respectively were firstly fabricated. To demonstrate that the fabricated SML-LMS-HE verily had a decreasing pore radius, scanning electron microscope (SEM) images of the cross sections for SML-LMS-HE were obtained. As shown in Fig. 2B, the SML-LMS-HE electrode was designed with larger pores in the middle and smaller pores on sides. Research has confirmed that SML-LMS-HE electrode could enhance the HER activity by inducing bubble splitting. For comparison, the typical dissociation process of bubbles with various diameters from SML-LMS-HE, MMM-MMM-HE and LMS-SML-HE were visualized, just as shown in Figs. 2C-F, H-K and M-P, respectively. Moreover, the diameter distributions of hydrogen bubbles ejecting from SML-LMS-HE (Fig. 2G), MMM-MMM-HE (Fig. 2L) and LMS-SML-HE (Fig. 2Q) were also displayed. It is found that the average diameter of bubbles releasing from SML-LMS-HE (74.5 μm) is smaller than that

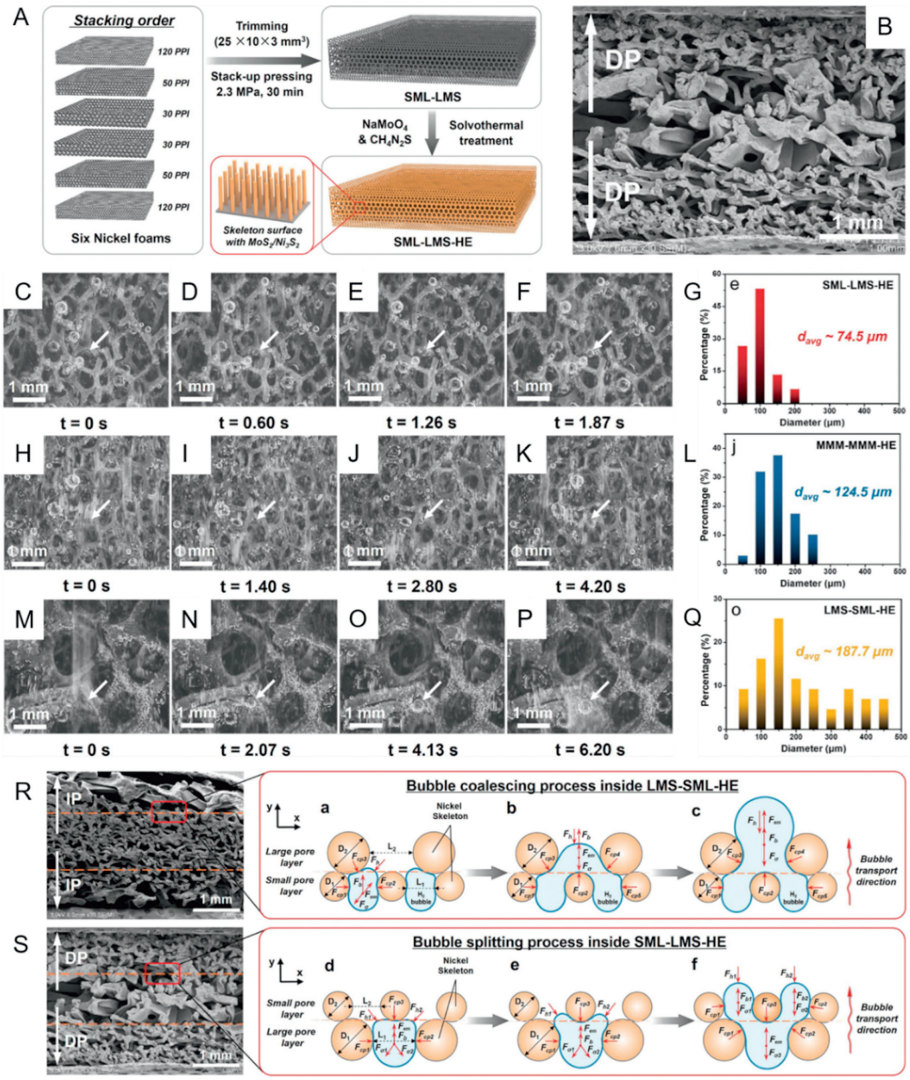

Fig. 2. (A) Schematic illustration of the production process of SML-LMS-HE. The 120, 50 and 30 PPI means the nickel foams with 120, 50 and 30 pores per linear inch. (B) Scanning electron microscope (SEM) images of cross sections of SML-LMS-HE. Sets of photographs for the typical bubble release process from the surface of SML-LMS-HE (C-F), MMM-MMM-HE (H-K) and LMS-SML-HE (M-P). The diameter distributions of hydrogen bubbles ejecting from SML-LMS-HE (G), MMM-MMM-HE (L) and LMS-SML-HE (Q). (R) The bubble coalescing process in LMS-SML-HE. (S) The bubble splitting process in SML-LMS-HE. Reprinted with permission [101]. Copyright 2022, Elsevier.

of MMM-MMM-HE (124.5 μm) and LMS-SML-HE (187.7 μm). The smaller bubble diameter means lower gas-phase occupancy and higher exposure rate of active areas, which indicates higher HER activity. To explain how this structure works, a force analysis near the critical point of bubble scale change is introduced. After a series of approximations, it is found that the surface tension force in the *y*-direction (F_{ad}), serving as the adhesion force, plays a key role in bubble transporting. According to the formula, the adhesion force is proportional to the diameters of the pore size (L) and nickel skeleton (D). Thus, as shown in Fig. 2R, the smaller bubbles tend to coalesce into larger ones when moving from the middle to the sides inside LMS-SML-HE due to the increasing adhesion forces which are dependent on the increasing pore size and nickel skeleton. In contrast, the larger bubbles tend to split into smaller bubbles when migrating from the middle to the sides inside SML-LMS-HE (Fig. 2S), where the diameters of pore size and nickel skeleton decrease from the middle to sides. The differences in structure influence the adhesion force during bubble transporting, resulting in different average bubble detachment diameters and then different amounts of exposed active sites, which eventually affect HER activity. To conclude, the gradient porous electrode (SML-LMS-HE) inducing bubble splitting exhibited a much higher bubble desorption rate than other electrodes, ensuring a high HER activity and durability. This novel gradient porous electrode provides a possible strategy to construct an electrocatalytic electrode with high performance for electrolysis of water to produce hydrogen.

3.2. Chevrel phase $CuMo_6S_8$/Cu electrode

Since the traditional electrode preparation technology adopts polymer adhesive or spraying, additional charge transfer resistance is generated and the catalyst is liable to drop off from the substrate when operating at high current density. *In-situ* growth of electrocatalyst nanoarrays on highly conductive substrates has become a new solution. Through dual interfacial engineering, Liu *et al.* synthesized a Chevrel phase $CuMo_6S_8$/Cu electrode with superior mechanical stability and HER performance [102]. The integrated structure of the electrode is achieved by loading the MoS_2 ink on the treated Cu foams by drop casting or spray coating and then annealing at 750 °C under Ar and H_2 atmosphere. Notably, the annealing process leads to the reaction between Cu atoms and MoS_2, *in-situ* forming Chevrel phase $CuMo_6S_8$ with porous struc-

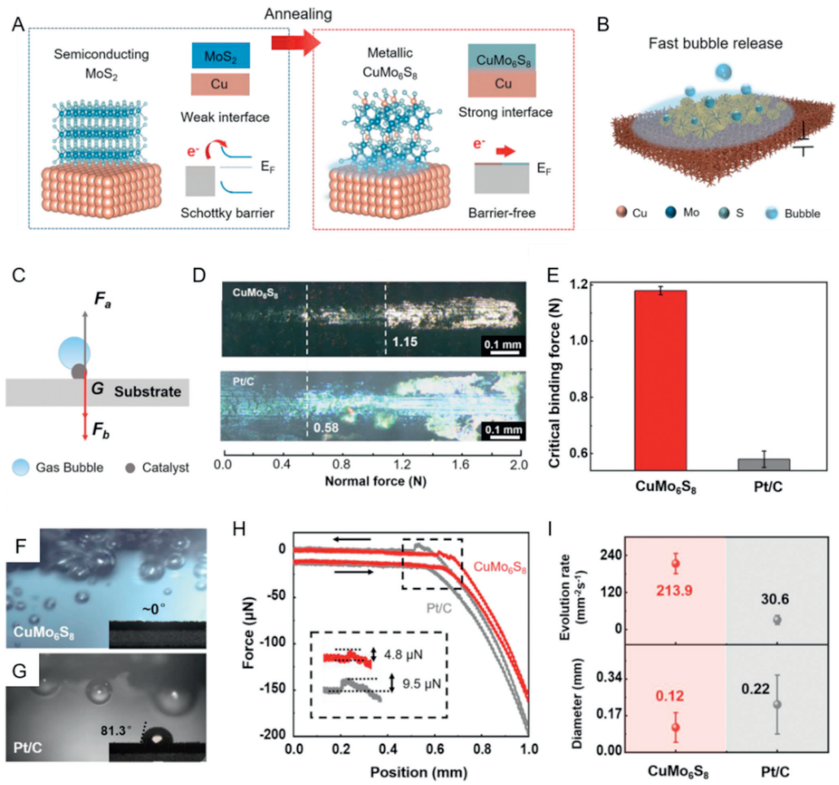

Fig. 3. (A, B) A schematic showing the preparation process and macro-performance of $CuMo_6S_8$/Cu electrode. (C) Force analysis model of gas bubbles attached on the electrode. F_a, F_b and G represent the electrocatalyst-bubble interfacial adhesion force, the electrocatalyst-support interfacial binding force, and the gravity of electrocatalysts, respectively. (D) The photos of micro-scratches of $CuMo_6S_8$ (top), Pt/C (bottom) catalyst layers adhesive on Cu foils. The dotted lines represent the critical adhesive forces corresponding catalysts. (E) The statistical data of critical adhesive forces of $CuMo_6S_8$ and Pt/C. The error bars represent the statistical distribution of three samples. The photos of gas bubbles generated on (F) $CuMo_6S_8$ and (G) Pt/C electrodes at 10 mA/cm^2. The insets show the corresponding contact angles of ~0° and 81.3° (H) Electrocatalyst-bubble interfacial adhesion force of $CuMo_6S_8$/Cu and Pt/C electrodes. (I) Evolution rate and diameter of gas bubbles of $CuMo_6S_8$ and Pt/C electrodes. The error bars represent the distribution of statistical values. Reprinted with permission [102]. Copyright 2022, Springer Nature.

ture. The chemical bonding between $CuMo_6S_8$ and Cu not only eliminates the Schottky barrier but also causes the tight binding of the catalyst and the support (Fig. 3A). What is more, the electrode exhibits the Wenzel-state wetting property (Fig. 3B), facilitating the release of H_2 bubbles and realizing the electrode working stably at 2500 mA/cm^2 for over 100 h. As shown in Fig. 3C, the electrocatalyst-bubble interfacial adhesion force and the electrocatalyst-support interfacial binding force is very important for the HER performance and catalyst stability. Quantitative analysis of these two forces is helpful to reveal the HER mechanism. According to Figs. 3D and E, it can be seen that $CuMo_6S_8$ electrode has stronger interfacial binding forces (1.15 N) than that of Pt/C electrode (0.58 N), which is conducive for the electrode to hold the structure when generating a large number of bubbles. The bubble evolution which happened on the electrode was observed with the help of optical microscopy. Figs. 3F and G show that the contact angle of $CuMo_6S_8$ is closely to 0° and the bubbles are smaller on $CuMo_6S_8$ electrode, which indicates that $CuMo_6S_8$ electrode is superhydrophilic and gas bubbles tend to detach from the electrode. This phenomenon could be further clearly illustrated through the electrocatalyst-bubble interfacial adhesion force test. As shown in Fig. 3H, the adhesion force of $CuMo_6S_8$/Cu electrode (9.5 μN) is much smaller than that of the Pt/C electrode (4.8 μN). These strengths are corresponded with the outstanding performance of the $CuMo_6S_8$ in terms of the evolution rate and diameter of gas bubbles in Fig. 3I. In general, the integrated electrode synthesized by *in-situ* growth method could solve the problems existing in traditional electrode preparation from the point of dual-interface engineering.

3.3. Superaerophilic/superaerophobic cooperative electrode

The release of bubbles could be described as detaching from the electrode surface and removed from the electrolyte, which greatly affect the efficiency of the reaction. To solve the negative effects caused by the bubbles slowly removed from the reaction system, developing a novel electrode to change the bubble removal way, thus promoting the mass transfer, is getting more and more attention.

Zhang *et al.* have constructed a superaerophilic/superaerophobic (SAL/SAB) cooperative electrode consisting of SAL stripes and SAB electrocatalytic regions, which can boost mass transfer efficiently by inducing fast bubble detachment and efficient dissolved H_2 diffusion [103]. Firstly, the SAL/flat Pt electrode is introduced to clarify the mechanism of the electrode structure. The device is mainly composed of a SAL/flat Pt electrode and a H_2 collector (Fig. 4A). When the H_2 bubbles generate on the Pt region at the beginning, the size of bubbles limits their contact with the SAL stripe, and the dissolved H_2 can disengage from the reaction system through gas cushion on the SAL stripe (Fig. 4B). As they grow, H_2 bubbles will contact the SAL stripes and then be driven to the H_2 collector (Fig. 4C). Owing to the gas cushion, the H_2 diffusion distance is greatly reduced, resulting in the enhanced diffusion efficiency. Meanwhile, the contacted bubbles can be timely transferred through SAL stripes under the drive of asymmetric Laplace pressure. Because of enhanced bubble detachment and dissolved H_2 diffusion, there are more exposed active sites for HER, thus effectively improving the reaction efficiency. To further explore the influence of various factors on improving reaction efficiency, the

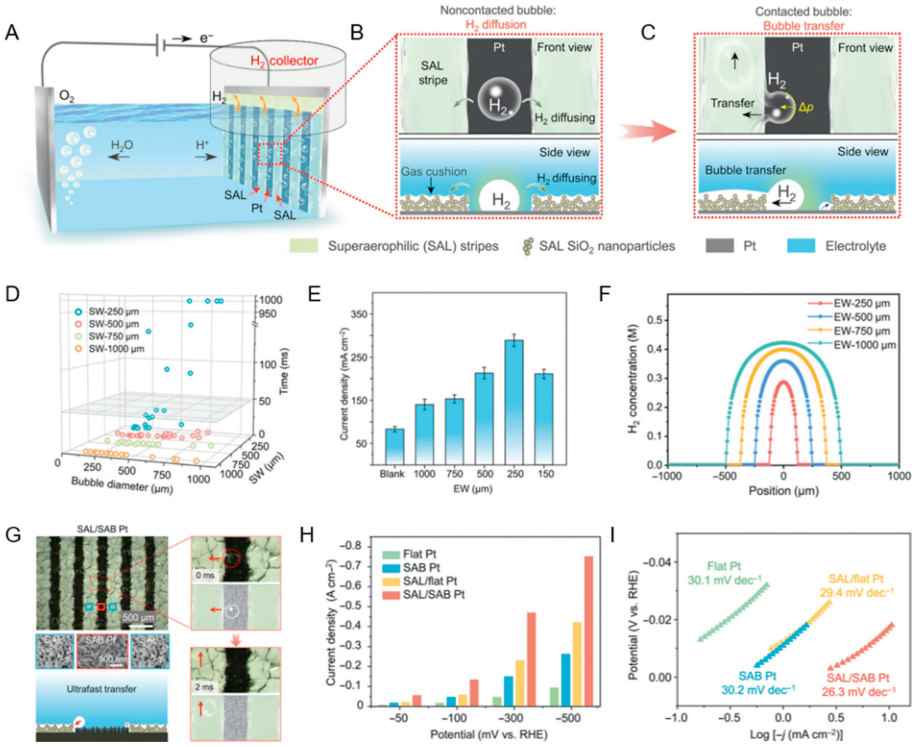

Fig. 4. (A) Schematic of the superaerophilic (SAL) /flat Pt electrode with enhanced mass transfer. (B) H_2 bubbles are not making contact with the SAL stripe. (C) As they grow, H_2 bubbles will contact the SAL stripes and be timely transferred through SAL stripes. (D) Statistics of the transfer time of H_2 bubbles with different diameters on the SAL stripes with various SAL stripe widths (SWs). (E) Variation of the current density of the SAL/flat Pt electrodes with various electrode widths (EWs) at an overpotential of −350 mV. (F) Simulation of H_2 diffusion on the SAL/flat Pt electrodes with various EWs. (G) H_2 bubble behaviors and electrochemical tests on the SAL/superaerophobic (SAB) Pt electrode. (H) Current densities of these four electrodes at −50, −100, −300 and −500 mV *vs.* RHE. (I) Tafel plots of these four electrodes. Reprinted with permission [103]. Copyright 2023, Wiley VCH.

SAL stripe width (SW) and electrode width (EW) are changed respectively. Fig. 4D shows the close connections between SW and H_2 bubbles' transfer efficiency. It was found that the larger SW will result in faster bubble transfer. Additionally, the diameter of the H_2 bubble determines the transfer efficiency as well. According to the mathematical formula, smaller bubble sizes and larger SWs will lead to a bigger pressure difference, which can enhance bubble transfer. However, the SW cannot be set too high, considering the electrode surface utilization. Besides SW, the EW also plays an important role in bubble transfer. As shown in Fig. 4E, the current densities increase with the decrease of EW, indicating enhanced HER efficiency. However, an EW of less than 250 μm is not taken because adjacent gas cushions will coalesce in this case. The significant enhancement of efficiency is mainly due to minor EW inducing diffusion of dissolved H_2. It can be learned from Fig. 4F that the peak H_2 concentration decreases with the reduction of EW. By adjusting the SW and EW properly, the promoting effect of electrode on the HER efficiency can be further improved. Through the modification of the electrode, the introduction of SAL stripes could enhance the mass transfer and provide a new way for diffusion of the dissolved H_2, but it can only transfer partial H_2 bubbles that cover in the flat Pt electrode. This is caused by the large adhesive force of flat Pt (~143 μN) to H_2 bubbles. Taken this issue, the wettability of the electrode could not be neglected, so nanostructured Pt with superaerophobicity is adapted (Fig. 4G). There is a low adhesive force attributed to the superaerophobicity of nanostructures, so the generated H_2 bubbles tend to disengage from the electrode and realize being transferred through the SAL stripes in 2 ms. In addition, current densities were measured at various overpotentials to characterize the HER performances. As shown in the histogram (Fig. 4H), there is a stark contrast at high overpotentials that the SAL/SAB Pt electrode exhibits a superior performance almost 5 times more than the flat Pt electrode. The similar Tafel slope of the SAL/SAB Pt electrode in Fig. 4I represents the reaction mechanism changes nothing but better than before. In summary, the construction of electrodes combining the SAL interface and the SAB interface has become a new strategy to reduce the bubble coverage on the electrode surface and accelerate the desorption of bubbles.

4. External fields imposing

Since the bubble itself is difficult to attach from the electrode and the electrolyte, external energy can be injected to promote bubble detachment. The simplest strategy of imposing external field at the laboratory level is agitation. However, this straightforward but crude strategy is highly energy-intensive that does not even consume enough energy to match the amount of hydrogen produced. In response to this problem, other forms of energy besides mechanical agitation have been developed to accelerate bubble detachment, including acoustic field [33,34,39,42], magnetic field [36,38,40,41], and supergravity field [55].

4.1. Acoustic field

Integrating ultrasound into the photocatalytic and electrocatalytic hydrogen production system was found to be effective for hydrogen production [104–110]. It has been reported that the acoustic field can accelerate the bubble detachment in electrocatalytic water splitting [33,34,39,111]. However, how to integrate ultrasound into electrocatalytic water splitting device reasonably and explore the its influence on HER performance deserves more attention. It is noteworthy that Ehrnst *et al.* [42] developed a

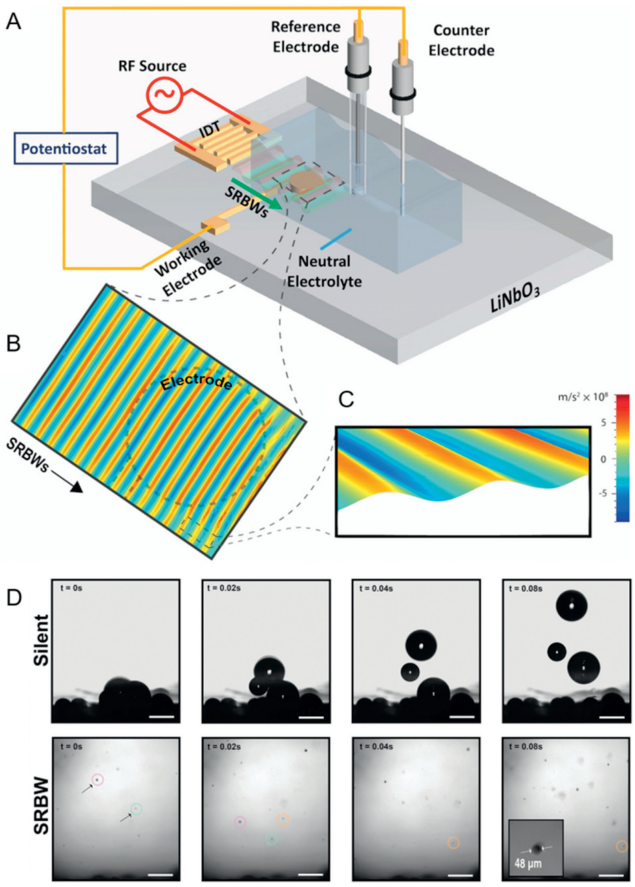

Fig. 5. (A) Schematic depiction (not to scale) of the SRBW electrochemical cell. (B, C) Laser Doppler vibrometry scans of the SRBWs (20 dBm) propagating on the $LiNbO_3$ substrate and through the WE (dashed outline); the color bar denotes the magnitude of the surface acceleration associated with the SRBW. (D) Representative time series images acquired using a high-speed camera (10,000 frames/s) showing the growth of bubbles trapped at the electrodes under silent conditions (top row), and under SRBW excitation at 20 dBm (bottom row). Identical bubbles are labeled by circles of the same color and the scale bars denote a length of 500 µm. Reprinted with permission [42]. Copyright 2022, Wiley VCH.

novel electrolysis technique driven by acoustic waves. They designed surface reflected bulk waves (SRBW) electrochemical cell shown in Figs. 5A-C, which consists of a glass electrolyte chamber containing a neutral electrolyte (0.1 mol/L sodium phosphate Na_2HPO_4/NaH_2PO_4) placed on a chipscale SRBW device. The device comprises a piezoelectric ($LiNbO_3$) substrate on which a digital intertransducer (IDT) electrode is located and the electrochemical setup is accomplished by an Ag/AgCl reference electrode (RE) and a platinum (Pt) line counter electrode (CE) mounted on the chamber cover. They experimented by using nanoscale MHz-order electromechanical oscillations in a unique mixed surface form and bulk sound waves called surface reflected bulk waves, demonstrated that the HER performance improves remarkably in neutral electrolytes on polycrystalline gold (Au) electrodes. The effect of acoustic waves on bubbles is one of the significant reasons for the improvement of HER performance. At high current densities, bubbles can accumulate on the electrode, hindering the electrode contact with water, and slowing down the reaction rate. Nevertheless, SRBW can facilitate the separation and removal of bubbles. As shown in Fig. 5D, under silent conditions, when the bubbles accumulated on the electrode grow to a diameter of approximately 450 µm, its buoyancy will be greater than the adsorption force, and the bubble will escape from the surface. However, under the condition of SRBW excitation at 20 dBm, not only is the critical bubble size (about 40 µm) before detachment an order of magnitude smaller than that in silent condition, but also bubbles can be eliminated before the further growth and fusion, which will limit the bubble aggregation on the electrode, thus speeding up the electrolysis process and significantly improving its conductivity and stability, facilitating the production of hydrogen. The lower frequency (from 20 kHz to 3 MHz) surface reflected bulk wave was used in the experiment, while the higher MHz frequency acoustic wave excitation was more beneficial to reduce the electrode surface degradation caused by bubble pitting. Additionally, compared with most current electrolytic devices using Pt as the electrode and strong acid or strong alkaline solution as the electrolyte, the SRBW electrochemical battery uses low-cost electrodes (such as polycrystalline gold and silver) and neutral electrolyte with low corrosion, immensely reducing the cost of electrolytic materials, and has a wide range of application prospects. However, SRBW electrochemical cells require additional energy consumption and complex setup, and their large-scale application requires large-scale nanofabricating technology as the foundation, so the problem of how to scale up the operation still needs to be solved. Moreover, the strategy may damage the structure of the catalyst, or even cause the catalyst to fall off. Therefore, it is significant to develop a more advanced ultrasonic strategy to achieve bubble detachment at micro scale and reveal the detachment mechanism.

4.2. Magnetic field

Compared with many other external fields, imposing external magnetic field is a simple and economical method to enhance the electrochemical gas evolution reactions by facilitating the detachment of generated gas bubbles from the electrode and accelerating the mass transfer of paramagnetic materials [32,37,40,112,113], which can be realized by only an ordinary permanent magnet and requires no additional energy input [38].

Through employing a magnet outside the electrode, Wang *et al.* [36] successfully removed the generated bubbles from the electrode surface and revealed the mechanism of bubble transport in the magnetic field. Under normal circumstances, a great amount of oxygen bubbles are produced and keep growing on the surface of anode during OER, among which the large bubbles will leave and gradually rise to the electrolyte surface, whereas the small bubbles will still remain on the electrode surface or in the electrolyte, covering the active sites and reducing the electrolyte conductivity (Fig. 6A). After the introduction of magnetic field, oxygen bubbles can be driven directionally (Fig. 6B), and the push of oxygen bubbles would in turn intensify electrolyte dynamics, contributing to faster detachment of bubbles. Afterwards, the magnetic field intensity was controlled to further investigate the influence of the magnetic field to OER. It was found that the electrolytic threshold can be effectively reduced with the increase of the magnetic field intensity, and the cell voltage were apparently more stable under circumstance of magnetic field, which indicates that the oxygen bubble detachment was accelerated. Similarly, it was also found that hydrogen bubbles can be propelled by magnetic field, whose movement was, nevertheless, in opposite to that of oxygen bubbles. On purpose of uncovering the mechanism of directional deflection motion of gas bubbles, numerous comparative experiments were implemented. It was only when the magnetic field and electric field existed simultaneously and the magnetic pole was parallel with the electrode surface that the generated gas bubbles can be driven. In essence, anions and cations in the electrolyte would respectively aggregate around the anodes and the cathode due to the electric field. Gas bubbles detached from the electrode surface and moved upward to the electrolyte surface, which means the ions on the surface of the bubbles moved at the same time, ion current coming into being consequently (Fig. 6C). As the mag-

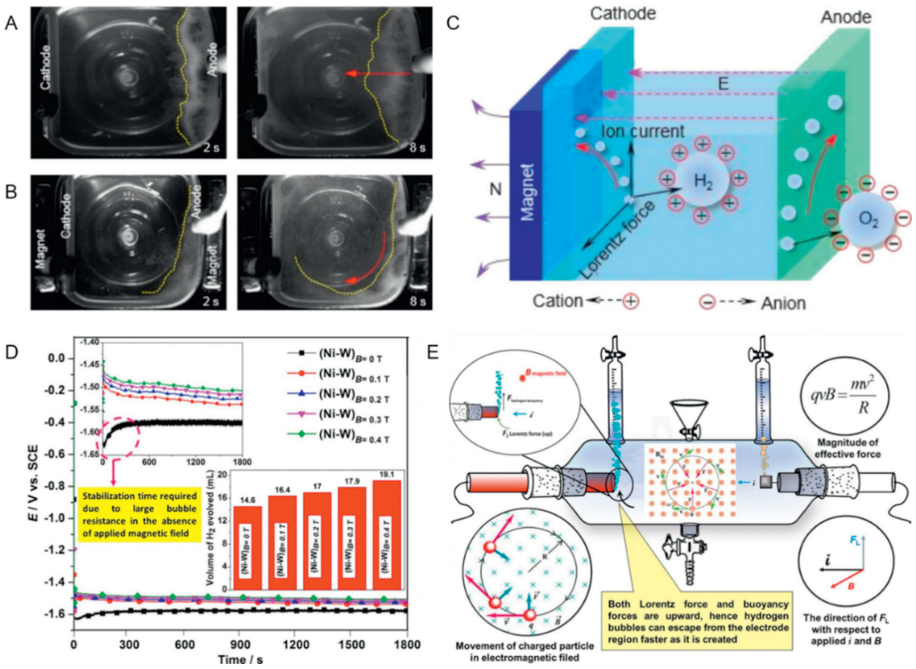

Fig. 6. (A) Diffusive movement of oxygen bubbles without magnet and (B) directional rotation movement of oxygen bubbles with magnet. (C) Mechanism of gas bubble movement in magnetic field. Reprinted with permission [36]. Copyright 2020, American Chemical Society. (D) The CP curves along with the quantified amount of H_2 evolved during the analysis (for 300 s). (E) The mechanism of enhancement in HER in the presence of applied magnetic field in perpendicular direction induced by Lorentz force acting in the same direction of the H_2 buoyancy force. Reprinted with permission [41]. Copyright 2017, Springer Nature.

netic field was perpendicular to the direction of the ion current, bubbles deflected directionally on account of correspond Lorentz force. In addition, the electrolyte can also be propelled due to the rotational motion of bubbles, creating a virtuous circle. Moreover, utilizing an electromagnet, Elias *et al.* [41] also imposed external magnetic field (0.1–0.4 T) in HER on a copper rod with Ni-W alloy coating and found the enhancement in HER efficiency. According to Fig. 6D, it was the large bubble resistance that led to a steady state before continuous hydrogen evolution without external magnetic field. In comparison, there was no such phenomenon with applied magnetic field, owing to the accelerated bubble detachment. In essence, bubbles can sperate from each other more quickly due to the convection produced by the Lorentz force driven motion of charged particles (Fig. 6E). With the combined effect of both Lorentz force and buoyancy, it takes a shorter time for bubbles to escape from the electrode surface.

To sum up, imposing external magnetic field is a novel method to facilitate bubble detachment by exerting Lorentz force on bubbles. However, the introduction of magnetic field by a permanent magnet may not satisfy the demand for electrocatalytic water splitting on large scale, and extra energy is inevitably required for the better efficiency.

4.3. Supergravity field

The supergravity field has been used in many fields because it could accelerate the interphase slip velocity, and has the advantages of easy maintenance, low energy consumption, safety and so on [114]. Since the bubbles have difficulty disengaging from the electrolytic system timely under normal gravity condition, it would result in the active sites being covered and the increase of the Ohmic resistance. Therefore, the researches on supergravity field applying to facilitate the disengagement of the gas bubbles have been carried out [81,95–97].

Wang *et al.* studied the effect of supergravity field (achieved by centrifuging with a cylindrical electrolytic cell) on bubbles and HER performance in 10% NaOH and 1.5 g/L sodium dodecylsulfonate (SDS) [55]. As shown in Fig. 7A, since the bubbles cannot be removed rapidly from the electrolysis system, it will be easy for them to combine with the surfactant (SDS) and produce hydrogen foam attached to the electrolyte surface, further hindering the detachment of bubbles. In supergravity conditions, it can be seen that the hydrogen foam in the central region gradually decreases with the increase of gravity coefficient (G) value, and finally can been seen only around the edges of the electrolytic cell. This phenomenon is directly reflected in the reduce of Ohmic resistance, which can be summarized as a relationship between Ohmic resistance reduction and log$G$, and then the function about G value and Ohmic voltage drop reduction ($i\Delta R_G$) can be obtained. It can be seen in Fig. 7B that as the G value increases, the $i\Delta R_G$ gradually increases. It is noteworthy that with the increase of current densities, $i\Delta R_G$ grows dramatically, which accounts for more intense effect of the supergravity field on the disengagement of bubbles from the electrolytic system. By conducting the current test (Fig. 7C), the current density is found to be proportional with the G value, demonstrating the enhanced effect on water electrolysis for hydrogen production. Besides, from Fig. 7D, it can be found that the cell voltage reduction (ΔU_G) was 0.51 V at 0.5 A/cm^2 under G value of 161. For a 100 kA electrolytic cell centrifuge designed in industrial, the energy consumption of achieving a supergravity field with G value of 161 only needs 3 kW, while it can potentially reduce 51 kW power supply. Therefore, the energy saving of hydrogen production by water electrolysis is much larger than sustaining a supergravity field. In a word, it is feasible to achieve rapid disengagement of bubbles with the external gravity field, improving the HER performance by increasing the interphase slip velocity. In addition, hydrogen production in low-gravity conditions is also worthy being further investigated. According to the previous research, under a low-gravity condition, due to the slow interphase slip velocity, the generated bubbles will adhere to the electrode surface and form gas bubble froth layers, which seriously affects the ion and gas transport at electrodes. As reported by Brinkert

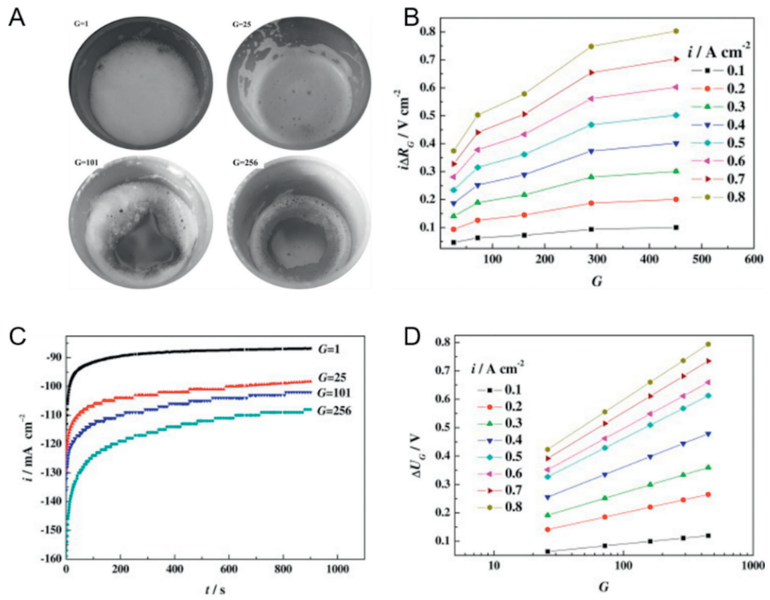

Fig. 7. (A) The states of hydrogen foam in electrolyte after chronoamperometry measurement under various gravity. (B) The Ohmic voltage drop reduction ($i\Delta R_G$) as a function of G value at various current densities. (C) Chronoamperometry curves for HER under various gravity conditions. (D) Cell voltage reduction (ΔU_G) as a function of G value at various current densities for water electrolysis. Reprinted with permission [55]. Copyright 2010, Elsevier.

et al. [115], through controlling the micro and nano topography of the Rh electrocatalyst, the electrolytic structure is adjusted to overcome the problems appeared in hydrogen production under a low-gravity condition. The research in this regard will promote the hydrogen production in the outer space and is expected to improve and extend life support systems for long-term space flights in the future.

5. System upgrade

The problems bubbles bring about in electrocatalytic water splitting can be mitigated or even solved through upgrading the system for the reaction [44–49]. Instead of detaching from the electrolyte, the generated gas bubbles can be collected more efficiently so that the residence time of bubbles in the electrocatalytic water splitting cell can be tremendously reduced, thus alleviating the impact of bubbles on the reaction performance [47]. Moreover, as a novel strategy, converting a system with a three-phase interface to a system with a two-phase can remove the existence of bubbles [48,49], thus avoiding the bubble negative effect.

5.1. Photothermal-electrocatalytic water vapor splitting device

In traditional electrocatalytic water splitting devices, the generated gas bubbles nucleate and gather at the electrode surface, failing to escape from the system timely, which blocks the active site on the surface of the electrode and then does harm to the performance of HER. The bubbles on the electrode surface and in the electrolyte make the performance fail to be fully utilized and will cause larger energy consumption in practical mass production. Fortunately, Zhang *et al.* [46] recently innovatively put forward an electrocatalytic water vapor splitting device from the perspective of changing the electrolysis system. Photothermal-electrocatalytic water vapor splitting device is different from the traditional electrocatalytic water splitting devices essentially. The detachment of bubbles from the electrode and electrolyte can be absolutely avoided.

The diagrammatic sketch of the electrocatalytic water vapor splitting device based on the wood structure is shown in Fig. 8A. The inset is the schematic illustration of the electrocatalytic water vapor splitting device configuration, in which the prepared electrocatalysts with lattice matched Mo_2C-Mo_2N heterointerfaces serves as cathodic electrocatalyst and commercial IrO_2 acts as the anodic electrocatalyst. A wood with carbonized surface was adopted as the photothermal material to efficiently generate water vapor. On account of its natural aligned microchannels, surface carbonized wood has fabulous light adsorption and transpiration effect, ensuring an excellent solar-to-steam efficiency. As depicted in Fig. 8B, the photograph of the electrode after water splitting is wet compared with that of the electrode before water splitting, which indicates that the photothermal-electrocatalytic water vapor splitting device was set up successfully. More detailed mechanism of water vapor splitting is shown in Fig. 8C, the vapor transformed by the photothermal effect could be reached at the electrode and was split into oxygen on the anode and hydrogen on the cathode. Polarization curves of electrolyzer adopting Mo_2C-Mo_2N heterostructures as HER electrocatalyst show the electrolysis performance of water vapor splitting is much superior than that of liquid water splitting (Fig. 8D). A series of HER catalysts were utilized to demonstrate that the performance of water vapor splitting is always better that of liquid water splitting (Fig. 8E). The density functional theory (DFT) was conducted to illustrate the HER mechanism at the atomic and molecular level. For the liquid phase, it was found that the free energy correspondingly decreases with the increase of temperature (Fig. 8F). Besides, at the same temperature, the free energy for gas phase is lower than that for liquid phase (Fig. 8G). Above all, water vapor splitting is much easier than liquid water splitting. According to Chapman-Enskog's theory, the diffusion coefficient of H_2 in the gas phase is larger than that in water, the friction resistance is lower, and it is easier to detach from the surface of the electrocatalyst, which makes the bubble adhere to the electrode surface, and the probability of blocking the active site from participating in the reaction is greatly reduced, thus greatly improving the HER performance of the device. To sum up, the electrocatalytic water vapor splitting device optimizes the electrolysis system, innovates the idea of HER, and ingeniously solves the bubble problem. To sum up, the electrocatalytic water vapor splitting device optimizes the electrolysis system, innovates the idea of HER, and ingeniously solves the bubble problem.

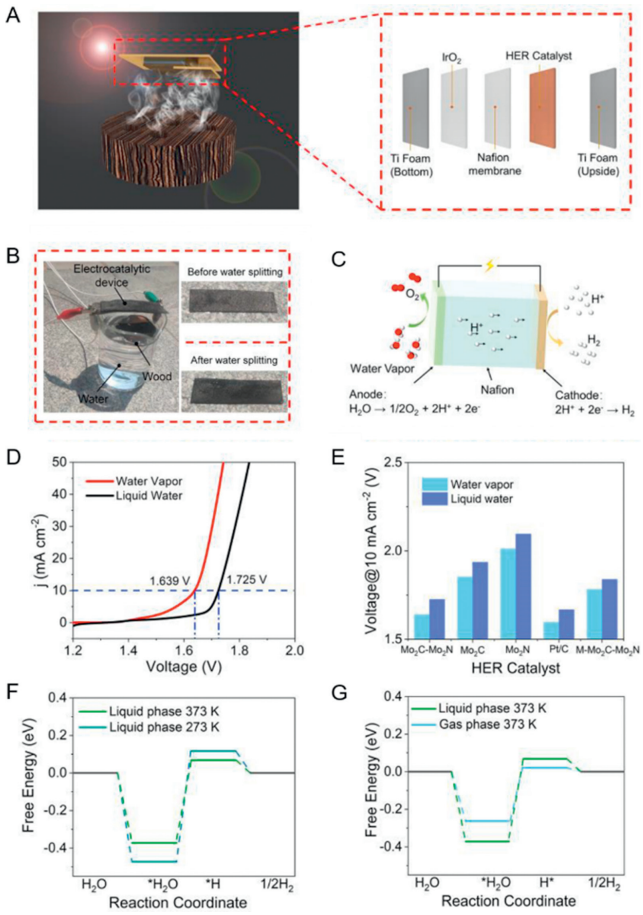

Fig. 8. (A) The diagrammatic sketch of the electrocatalytic water vapor splitting device based on the wood structure. The inset is the schematic illustration of the electrocatalytic water vapor splitting device configuration. (B) Photograph of the setup for the electrocatalytic steam splitting. Insets are the photographs of setup before and after water splitting. (C) Sketch of the mechanism of the water vapor splitting electrolyzer. (D) Polarization curves of electrolyzer adopting Mo_2C-Mo_2N heterostructures as HER electrocatalyst at a scan rate of 5 mV/s in the vapor phase and liquid phase, respectively. (E) Summaries of the voltage at 10 mA/cm^2 using the Mo_2C-Mo_2N, Mo_2C, Mo_2N, M-Mo_2C-Mo_2N and 20 wt% Pt/C as HER electrocatalyst in the liquid water and water vapor. (F) Free energy profiles of Mo_2C-Mo_2N heterostructures under different temperatures. (G) Free energy profiles of Mo_2C-Mo_2N heterostructures under different phase states. Reprinted with permission [46]. Copyright 2022, Wiley VCH.

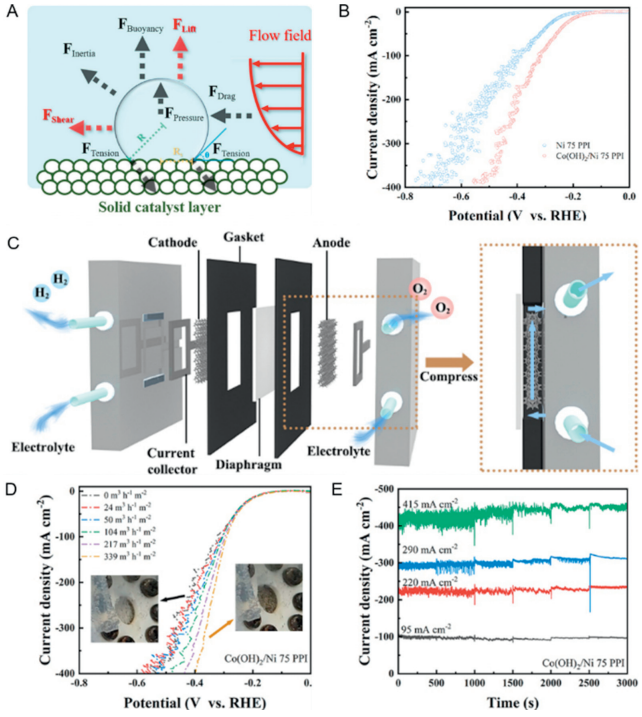

Fig. 9. (A) Force analysis of single bubble on electrode surface under forced convection flow field. Reprinted with permission [45]. Copyright 2022, Elsevier. (B) Polarization curves of Ni and $Co(OH)_2$/Ni electrodes. (C) Schematic of flow-through electrolyzer. (D) Linear sweep voltammetry (LSV) curves for $Co(OH)_2$/Ni flow-through electrode with a pore size of 75 PPI under different flux, insets are optical images of the electrode surface with flows (right) and without flows (left). (E) Chronoamperograms of $Co(OH)_2$/Ni flow-through electrodes with a pore size of 75 PPI under different current densities and different flux, the flux is increased every 500 s. Reprinted with permission [49]. Copyright 2022, Elsevier.

5.2. Flow-through electrodes

Flow-through electrode is wildly used in HER and is considered an efficient strategy to deal with negative effect of bubbles [116–122]. Bubble behavior could affect transport processes such as diffusion, convection, and migration, and ultimately change the overpotential. In general, it is quite difficult to remove bubbles in time without additional external force field. According to force analysis in Fig. 9A, both shear force and lift force act as the crucial roles in easier bubble detachment. Novel flow-through electrolyzer which can generate additional shear force and lift force on bubbles, is capable to optimize the bubble behavior, finally contributed to hydrogen evolution with high efficiency and stable performance.

Chen *et al.* [49] put forward a flow-through electrode with Co-based nanosheets immobilized on Ni foam for water splitting, which can effectively facilitate bubble detachment without additional equipment investment. Firstly, in order to intensify the roughness of electrode surface and weaken the adhesion which made lift force dominant between the electrode and generated bubble, both the internal and the external surface of the electrode were immobilized with the nanosheet-shaped $Co(OH)_2$. Although the overpotential bubble induced can be mitigated for the microstructure change in the pore surface, massive fluctuations do exist in linear sweep voltammetry (LSV) curves, especially under high current density (Fig. 9B), since the generated gas bubbles can be trapped in the pores and cannot be removed timely. On the purpose of further accelerating the detachment of generated bubbles, a novel electrolyzer assembled with flow-through electrode was developed, where the electrolyte flowing through the electrodes with interconnected pores, and the flowing electrolyte fluid caused shear force on bubbles. In the electrolyzer, a peristaltic pump was used to control the electrolyte flux, making the electrolyte recirculated in the corresponding compartment of the cell (Fig. 9C). As shown in Fig. 9D, compared to the electrode without flowing electrolyte, the overpotential of HER became lower when the pore size was fixed. Besides, with the increase of the electrolyte flux, the potential of HER correspondingly decreased. By calculation, it can be found that the potential of HER would show a tremendous decrease as the current densities increase at a fixed electrolyte flux, which can be attributed to the rapid detachment of generated gas bubbles. In addition, the decreases in potential of HER were more obvious by increasing the flux of electrolytes flowing. Moreover, it can be found that at different current density, the disturbance of current density can be gradually mitigated by continuously increasing the flux of electrolytes (Fig. 9E). Theoretically, a higher electrolyte flux would generate a greater shear force, which would reduce the residence time of generated bubbles in consequence. Therefore, bubbles can be removed quickly from the micro-grade pores and the catalyst active sites can be re-exposed.

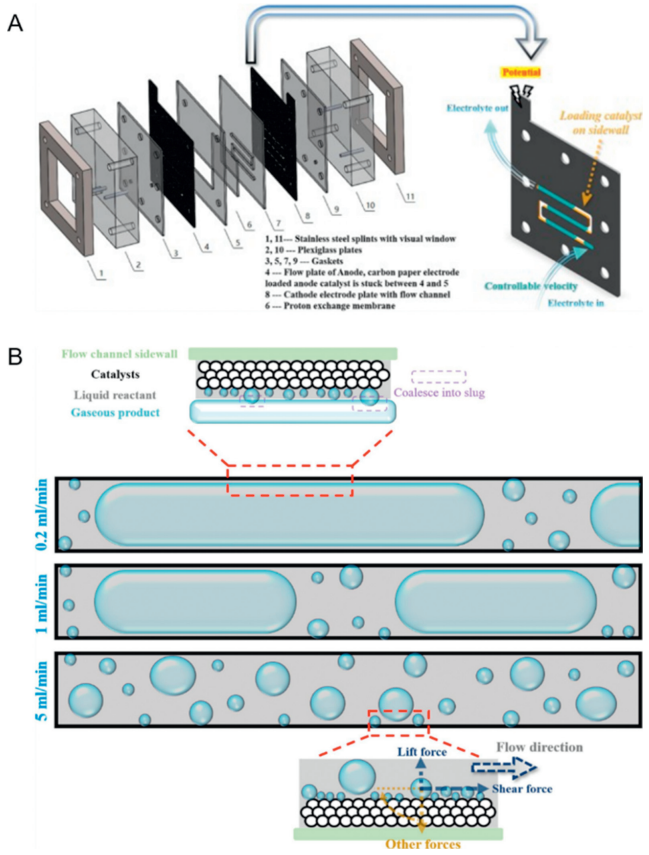

Fig. 10. (A) Assembly diagram of MER and illustration of cathode electrode plate with the flow channel. (B) Schematic illustration of different optimization mechanisms corresponding to different flow patterns. Reprinted with permission [45]. Copyright 2022, Elsevier.

Shi *et al.* [45] constructed a novel the microfluidic electrochemical reactor (MER) by promoting the electrode and the liquid flow path. The electrodes of the MER device (Fig. 10A) were prepared by spraying, and 0.2 mg/cm^2 catalysts were loaded on the side walls of the two electrode channels. A graphite plate with snake runner was used as the collector and cathode electrode, and Pt/C acted as the catalyst. For the anode, a planar electrode was used to demonstrate the fabulous performance of the cathode in a two-phase flow mode with forced convection. IrO_2 was used as catalyst and microporous carbon paper was used as its support. The two poles were separated by a Nafion-117 proton exchange membrane, and the layers of the device were closely connected with each other, then good air tightness was realized. To control the electrolyte flow, two peristaltic pumps with the same single-channel pump head were used in the liquid drive module. After multiple cyclic voltammetry (CV) tests and LSV tests, it is worth noting that although the microchannel electrode had a smaller electrochemical active surface area (ECSA), its overall Ohmic resistance was significantly lower than traditional H-cell with less energy loss, which is attributed to the compact and integrated character of the device. This abnormal phenomenon results from the optimized bubble behavior, and the velocity is an essential factor affecting the bubble behavior. In narrow passages, the effect of flow rate is amplified, and low flow rate causes gas to inevitably gather. In addition to the shielding effect of the gas slug, at the liquid slug, even if the reactant is sufficient, bubble escape at low flow rates is still unfavorable. Insufficient supply of reactants at the liquid film will still increase Ohmic overpotential and concentration overpotential, which fails to reach the expected effect. However, as the electrolyte flow rate increases in Fig. 10B, the length of the gas slug become shortened gradually, and the average current density increases in a stepped way. When the flow rate reached a high velocity of 5 mL/min, shear force and lift force are dominant forces to change the behavior of bubbles and shorten their growth cycle, making bubbles diffuse and shrink in size, then the blockings are unblocked. At high flow rates, mass transfer is strengthened. Meanwhile, both the average current density and current stability greatly improved. When the flow rate exceeds a certain threshold, the current density reaches saturation. The long-term stability the whole system showed during the 28 h operation at a high flow rate full confirmed its potential for industrial application.

In summary, the flow-through electrodes promote gas bubbles detachment and ameliorated the dynamics and mass transfer performance of the device, which greatly substantially reduces the Ohmic resistance of the system, realizing the obvious enhancement of HER performance and the reduction of energy loss. These new devices can be applied for not only water splitting, but also other gas evolution reactions to improve electrochemical performance. However, the pump work consumed in the flow strategy needs to be considered with the bubble removal saved energy to obtain optimal flow field parameters. Meanwhile, effective methods to mitigate the falling off of active substances on the electrode within the flow fields should be studied because of intense flow scouring vibration.

6. Conclusion and outlook

In previous sections, multiple strategies to facilitate bubble detachment and thereby mitigate the negative effects induced by bubbles were summarized from the aspects of electrode design, external field and system upgrading [123–128]. The principle, functional features, practicability, advantages and limitations of each strategy were also elaborated. With assistance of these advanced strategies, Ohmic overpotential and concentration overpotential can be effectively reduced, thus improving the efficiency of electrocatalytic water splitting. Although much progress has been achieved, there are still some unaddressed challenges holding the key to the future development of advanced bubbles detachment strategies for efficient hydrogen evolution:

(1) Under practical industrial conditions. The effect resulting from generated bubbles gathering on the electrode and staying in the electrolyte cannot be overlooked if hydrogen is to be produced at the industrial level. However, most of these strategies were adopted and evaluated under the laboratory condition and are not necessarily adapted to industrial high current density. Furthermore, no matter imposing external fields or modifying electrodes, it usually involves huge extra energy consumption and consequent large cost on the industrial scale. Only when the hydrogen energy obtained exceeds the energy consumption required do these strategies make sense in industrial applications.
(2) Seawater splitting. At present, the mature water electrolysis technology uses high purity water as raw material. Using large amounts of highly purified water to produce hydrogen could exacerbate freshwater shortages. Seawater, by contrast, making up 96.5% of the earth's water reserves, is an almost limitless resource and natural feedstock of electrolytes. However, due to the complexity of natural seawater, direct electrolysis of seawater is still in its infancy. The main problem lies in the low efficiency and poor stability of the electrolytic system under near-neutral conditions, and the existence of high concentration of harmful chloride ions and other cations (Mg^{2+} and $Ca2^{+}$) in seawater will not only lead to harmful chlorine oxidation/corrosion in practical operation, but also produce the

formation of a large number of insoluble precipitate (such as $Mg(OH)_2$), clogging the cathode physically

(3) Synergistic employment of multi-strategies. It is not uncommon to employ single strategy in electrocatalytic water splitting to promote bubble detachment. Nevertheless, synergistic employment of multi-strategies was rarely studied but has great potential for further bubble detachment boosting. Therefore, more research should focus on the combined influence of multi-strategies and their possible complex mutual interference. Overall, given that external fields are introduced to electrochemical systems, future development should be placed on the efficient and convenient integration of active strategies into electrochemical system.

(4) Artificial Intelligence assisted hydrogen production. Great progress has been made in the development of catalysts in electrocatalytic water splitting, and the performance of some catalysts can be even comparable to that of platinum-based catalysts. However, their stability and performance still cannot satisfy the industrial application under high current density, for many factors which make an impact on practical hydrogen production also exist, including bubble effect. In consequence, in addition to screening for high performance non-platinum catalysts, more research should be carried out to concentrate on bubble behaviors under different temperature, pressure and catalyst load, which takes huge amount of work and may well lead to a low work efficiency. In addition, while analyzing valuable experimental data, it is difficult for even experienced workers to directly correlate numerous variables of the high-dimensional model to draw universal conclusions and guide experimental work. The introduction of artificial intelligence (AI) into the design of industrial catalytic hydrogen-producing non-platinum catalysts can effectively solve this problem. Through this interdisciplinary technology integration of artificial intelligence and hydrogen energy, we can further understand the relationship between various parameters in the hydrogen production process, deepen our understanding of the hydrogen production process, and provide new development ideas for the further optimization of the hydrogen production process.

(5) Water splitting in outer space. Water splitting is a promising technology for human exploration in outer space because the produced oxygen is indispensable for human survival and the produced hydrogen could act as power source. It has been reported that several researches conducted water splitting under simulated Mars conditions (*i.e.*, Mars temperature and pressure). With the advance of astronautical technology, carrying out water splitting in real condition of outer space comes true.

Declaration of competing interest

The authors declare that they have no known competing financial interests or personal relationships that could have appeared to influence the work reported in this paper.

Acknowledgments

This work was financially supported by the National Natural Science Foundation of China (No. 51902101), the Youth Natural Science Foundation of Hunan Province (No. 2021JJ40044), Natural Science Foundation of Jiangsu Province (No. BK20201381), Science Foundation of Nanjing University of Posts and Telecommunications (Nos. NY219144 and NY221046), and the National College Student Innovation and Entrepreneurship Training Program (No. 202210293171 K).

References

[1] H. Ishaq, I. Dincer, C. Crawford, Int. J. Hydrog. Energy 47 (2022) 26238–26264.
[2] M. Younas, S. Shafique, A. Hafeez, F. Javed, F. Rehman, Fuel 316 (2022) 123317.
[3] A. Kovač, M. Paranos, D. Marciuš, Int. J. Hydrog. Energy 46 (2021) 10016–10035.
[4] T. Capurso, M. Stefanizzi, M. Torresi, S.M. Camporeale, Energ. Convers. Manag. 251 (2022) 114898.
[5] X. Li, L. Zhao, J. Yu, et al., Nano-Micro Lett. 12 (2020) 131.
[6] T. Terlouw, C. Bauer, R. McKenna, M. Mazzotti, Energy Environ. Sci. 15 (2022) 3583–3602.
[7] X. Xiao, L. Yang, W. Sun, et al., Small 18 (2022) 2105830.
[8] Z. Yu, Y. Duan, X. Feng, et al., Adv. Mater. 33 (2021) 2007100.
[9] Q. He, L. Wang, K. Yin, S. Luo, Nanoscale Res. Lett. 13 (2018) 167.
[10] M. Liu, H. Li, S. Liu, et al., Nano Res. 15 (2022) 5946–5952.
[11] Y. Li, Y. Sun, Y. Qin, et al., Adv. Energy Mater. 10 (2020) 1903120.
[12] Y. Fu, Y. Shan, G. Zhou, et al., Joule 3 (2019) 2955–2967.
[13] Y. Li, L. Wang, S. Zhang, et al., Catal. Sci. Technol. 7 (2017) 718–724.
[14] C. Chang, L. Wang, L. Xie, et al., Nano Res. 15 (2022) 8613–8635.
[15] R. Iwata, L. Zhang, K.L. Wilke, et al., Joule 5 (2021) 887–900.
[16] L. Chen, X. Zhang, A. Chen, et al., Chin. J. Catal. 43 (2022) 11–32.
[17] Y. Zeng, M. Zhao, Z. Huang, et al., Adv. Energy Mater. 12 (2022) 2201713.
[18] M. Jin, X. Zhang, S. Niu, et al., ACS Nano 16 (2022) 11577–11597.
[19] T. Guo, L. Li, Z. Wang, Adv. Energy Mater. 12 (2022) 2200827.
[20] A. Ali, F. Long, P. Shen, Electrochem. Energy Rev. 5 (2022) 1–30.
[21] K. Dastafkan, Q. Meyer, X. Chen, C. Zhao, Small 16 (2020) 2002412.
[22] P.A. Kempler, R.H. Coridan, N.S. Lewis, Energy Environ. Sci. 13 (2020) 1808–1817.
[23] T. Kou, S. Wang, R. Shi, et al., Adv. Energy Mater. 10 (2020) 2002955.
[24] S. Xu, Q. Wu, B. Lu, et al., Acta Phys. Chim. Sin. 39 (2022) 2209001.
[25] Y. Luo, Z. Zhang, M. Chhowalla, B. Liu, Adv. Mater. 34 (2022) 2108133.
[26] S. Ben, Y. Ning, Z. Zhao, et al., Adv. Funct. Mater. 32 (2022) 2113374.
[27] R.A. Márquez, K. Kawashima, Y.J. Son, et al., ACS Appl. Mater. Interfaces 14 (2022) 42153–42170.
[28] M. Jiang, H. Wang, Y. Li, et al., Small 13 (2017) 1602240.
[29] Y. Xu, X. Jiang, G. Shao, et al., Energy Environ. Mater. 4 (2021) 117–125.
[30] M. Liu, Z. Sun, S. Li, et al., J. Mater. Chem. A 9 (2021) 22129–22139.
[31] X. Li, Y. Jiang, Z. Zhang, et al., Colloid. Surface A 621 (2021) 126547.
[32] T. Iida, H. Matsushima, Y. Fukunaka, J. Electrochem. Soc. 154 (2007) E112.
[33] F. Foroughi, C. Immanuel Bernäcker, L. Röntzsch, B.G. Pollet, Ultrason. Sonochem. 84 (2022) 105979.
[34] S. Merouani, O. Hamdaoui, Ultrason. Sonochem. 32 (2016) 320–327.
[35] M. Wang, Z. Wang, Z. Guo, Z. Li, Int. J. Hydrog. Energy 36 (2011) 3305–3312.
[36] K. Wang, C. Liao, W. Wang, et al., ACS Appl. Energy Mater. 3 (2020) 6752–6757.
[37] Y. Zhang, C. Liang, J. Wu, et al., ACS Appl. Energy Mater. 3 (2020) 10303–10316.
[38] Y. Li, L. Zhang, J. Peng, W. Zhang, K. Peng, J. Power Sources 433 (2019) 226704.
[39] K.M. Cho, P.R. Deshmukh, W.G. Shin, Ultrason. Sonochem. 80 (2021) 105796.
[40] Y. Liu, L. Pan, H. Liu, et al., Int. J. Hydrog. Energy 44 (2019) 1352–1358.
[41] L. Elias, A.C. Hegde, Electrocatalysis 8 (2017) 375–382.
[42] Y. Ehrnst, P.C. Sherrell, A.R. Rezk, L.Y. Yeo, Adv. Energy Mater. 13 (2023) 2203164.
[43] X. Yin, G. Sun, A. Song, et al., Electrochim. Acta 249 (2017) 52–63.
[44] J. Zhang, F. Dong, C. Wang, et al., ACS Appl. Mater. Interfaces 13 (2021) 32435–32441.
[45] T. Shi, H. Feng, D. Liu, Y. Zhang, Q. Li, Appl. Energ. 325 (2022) 119887.
[46] Y. Zhang, P. Guo, S. Guo, et al., Angew. Chem. Int. Ed. 61 (2022) e202209703.
[47] H. Rox, A. Bashkatov, X. Yang, et al., Int. J. Hydrog. Energy 48 (2023) 2892–2905.
[48] A. Hodges, A.L. Hoang, G. Tsekouras, et al., Nat. Commun. 13 (2022) 1304.
[49] Y. Chen, J. Chen, K. Bai, Z. Xiao, S. Fan, J. Power Sources 561 (2023) 232733.
[50] N. Pande, G. Mul, D. Lohse, B. Mei, J. Electrochem. Soc. 166 (2019) E280.
[51] A.R. Zeradjanin, P. Narangoda, I. Spanos, J. Masa, R. Schlögl, Curr. Opin. Electrochem. 30 (2021) 100797.
[52] G.B. Darband, M. Aliofkhazraei, S. Shanmugam, Renew. Sustain. Energy Rev. 114 (2019) 109300.
[53] Z. Xie, S. Yu, G. Yang, et al., Chem. Eng. 410 (2021) 128333.
[54] Y. Li, H. Zhang, T. Xu, et al., Adv. Funct. Mater. 25 (2015) 1737–1744.
[55] M. Wang, Z. Wang, Z. Guo, Int. J. Hydrog. Energy 35 (2010) 3198–3205.
[56] X. Yu, M. Wang, Z. Wang, X. Gong, Z. Guo, J. Phys. Chem. C 121 (2017) 16792–16802.
[57] M. Bae, Y. Kang, D.W. Lee, D. Jeon, J. Ryu, Adv. Energy Mater. 12 (2022) 2201452.
[58] D. Jeon, J. Park, C. Shin, et al., Sci. Adv. 6 (2020) eaaz3944.
[59] B. Wu, T. Wang, B. Liu, et al., Nat. Commun. 13 (2022) 4460.
[60] W. Yin, Y. Cai, L. Xie, et al., Nano Res. 16 (2023) 4381–4398.
[61] Y. He, Y. Cui, W. Shang, Z. Zhao, P. Tan, Chem. Eng. J. 448 (2022) 137782.
[62] Y. He, Y. Cui, W. Shang, Z. Zhao, P. Tan, Chem. Eng. J. 438 (2022) 135541.
[63] J. Tan, B. Kang, K. Kim, et al., Nat. Energy 7 (2022) 537–547.
[64] Q. Song, Z. Xue, C. Liu, et al., J. Am. Chem. Soc. 142 (2020) 1857–1863.
[65] K. Torii, M. Kodama, S. Hirai, Int. J. Hydrog. Energy 46 (2021) 35088–35101.
[66] L. Jiang, N. Yang, C. Yang, et al., Appl. Catal. B: Environ. 269 (2020) 118780.
[67] Y. Tang, F. Liu, W. Liu, et al., Appl. Catal. B: Environ. 321 (2023) 122081.
[68] W. Xu, Z. Lu, P. Wan, Y. Kuang, X. Sun, Small 12 (2016) 2492–2498.
[69] J. Shen, B. Li, Y. Zheng, et al., Chem. Eng. J. 433 (2022) 133517.
[70] D. Wang, Y. Liu, L. Liu, et al., Nano Res. 16 (2023) 6584–6592.
[71] W. Liu, X. Wang, F. Wang, et al., Nat. Commun. 12 (2021) 6776.
[72] X. Xu, G. Fu, Y. Wang, et al., Nano Lett. 23 (2023) 629–636.

[73] O. van der Heijden, S. Park, J.J.J. Eggebeen, M.T.M. Koper, Angew. Chem. Int. Ed. 62 (2023) e202216477.
[74] G. Issabayeva, M.K. Aroua, N.M. Sulaiman, Desalination 194 (2006) 192–201.
[75] G.F. Swiegers, A.L. Hoang, A. Hodges, et al., Curr. Opin. Electrochem. 32 (2022) 100881.
[76] D. Huang, B. Xiong, J. Fang, et al., Appl. Energy 314 (2022) 118987.
[77] J. Zhou, M. Guo, L. Wang, et al., Chem. Eng. J. 366 (2019) 163–171.
[78] S. Wang, L. Wang, L. Xie, et al., Nano Res. 15 (2022) 4996–5003.
[79] L. Lin, P. Sherrell, Y. Liu, et al., Adv. Energy Mater. 10 (2020) 1903870.
[80] Y. Xu, L. Wang, X. Liu, et al., J. Mater. Chem. A 4 (2016) 16524–16530.
[81] A. Han, X. Zhou, X. Wang, et al., Nat. Commun. 12 (2021) 709.
[82] S. Zhang, L. Wang, C. Liu, et al., Water Res. 121 (2017) 11–19.
[83] L. Wang, X. Liu, Q. Zhang, et al., Nano Energy 61 (2019) 194–200.
[84] Q. Zhang, L. Wang, J. Wang, et al., J. Mater. Chem. A 6 (2018) 9411–9419.
[85] N. Han, K.R. Yang, Z. Lu, et al., Nat. Commun. 9 (2018) 924.
[86] J. Schröder, V.A. Mints, A. Bornet, et al., JACS Au 1 (2021) 247–251.
[87] X. Shan, J. Liu, H. Mu, et al., Angew. Chem. Int. Ed. 59 (2020) 1659–1665.
[88] J. Cao, J. Zhou, M. Li, et al., Chin. Chem. Lett. 33 (2022) 3745–3751.
[89] Q. Hu, Z. Wang, X. Huang, et al., Appl. Catal. B. Environ. 286 (2021) 119920.
[90] Z. Lu, Y. Li, X. Lei, J. Liu, X. Sun, Mater. Horiz. 2 (2015) 294–298.
[91] Z. Lu, W. Zhu, X. Yu, et al., Adv. Mater. 26 (2014) 2683–2687.
[92] L. Xie, L. Wang, W. Zhao, et al., Nat. Commun. 12 (2021) 5070.
[93] P. Lv, P. Peñas, H.Le The, et al., Phys. Rev. Lett. 127 (2021) 235501.
[94] G.F. Swiegers, R.N.L. Terrett, G. Tsekouras, et al., Sustain. Energ. Fuels 5 (2021) 1280–1310.
[95] X. Yu, X. Ren, Y. Zhang, et al., J. Mater. Sci. Technol. 65 (2021) 118–125.
[96] Y. Zhang, W. Cui, L. Li, et al., Int. J. Hydrog. Energy 47 (2022) 13552–13560.
[97] L. Wang, G. Zhou, H. Luo, et al., Appl. Catal. B: Environ. 256 (2019) 117802.
[98] Q. Cheng, M. Wang, J. Ni, et al., Carbon Energy 5 (2023) e307.
[99] X. Zhao, H. Ren, L. Luo, Langmuir 35 (2019) 5392–5408.
[100] L. Mattarozzi, S. Cattarin, N. Comisso, et al., Electrochim. Acta 140 (2014) 337–344.
[101] Y. Yang, J. Li, Y. Yang, et al., Appl. Energy 307 (2022) 118278.
[102] H. Liu, R. Xie, Y. Luo, et al., Nat. Commun. 13 (2022) 6382.
[103] C. Zhang, Z. Xu, N. Han, et al., Sci. Adv. 9 (2023) eadd6978.
[104] A.A. Yadav, Y.M. Hunge, S.W. Kang, Ultrason. Sonochem. 72 (2021) 105454.
[105] P.V. Cherepanov, M. Ashokkumar, D.V. Andreeva, Ultrason. Sonochem. 23 (2015) 142–147.
[106] S. Wang, R. Herrmann, A. Reiner, A. Wixforth, C. Westerhausen, Catal. Sci. Technol. 11 (2021) 1458–1466.
[107] N. Merabet, K. Kerboua, Int. J. Hydrog. Energy 47 (2022) 17879–17893.
[108] H. Abid, G. Rekhila, F. Ait Ihaddadene, Y. Bessekhouad, M. Trari, Int. J. Hydrog. Energy 44 (2019) 10301–10308.
[109] B.G. Pollet, F. Foroughi, A.Y. Faid, D.R. Emberson, M. Islam, Ultrason. Sonochem. 69 (2020) 105238.
[110] S. Guo, J. Su, H. Luo, et al., ACS Catal. 13 (2023) 296–307.
[111] X. Ma, T. Xing, B. Huang, Q. Li, Y. Yang, Ultrason. Sonochem. 40 (2018) 480–487.
[112] J. Yao, W. Huang, W. Fang, et al., Small Methods 4 (2020) 2000494.
[113] W. Zhou, M. Chen, M. Guo, et al., Nano Lett. 20 (2020) 2923–2930.
[114] M. Wang, Z. Wang, Z. Guo, Int. J. Hydrog. Energy 34 (2009) 5311–5317.
[115] K. Brinkert, M.H. Richter, Ö. Akay, et al., Nat. Commun. 9 (2018) 1–8.
[116] A.E. Angulo, D. Frey, M.A. Modestino, Energy Fuels 36 (2022) 7908–7914.
[117] M.I. Gillespie, F. van der Merwe, R.J. Kriek, J. Power Sources 293 (2015) 228–235.
[118] M.M. Saleh, Electrochim. Acta 45 (1999) 959–967.
[119] F. Rocha, R. Delmelle, C. Georgiadis, J. Proost, J. Environ. Chem. Eng. 10 (2022) 107648.
[120] Q. Lan, D. Ye, X. Zhu, et al., J. Power Sources 544 (2022) 231881.
[121] F. Yang, M.J. Kim, M. Brown, B.J. Wiley, Adv. Energy Mater. 10 (2020) 2001174.
[122] A. Maljusch, O. Conradi, S. Hoch, M. Blug, W. Schuhmann, Anal. Chem. 88 (2016) 7597–7602.
[123] Z. Ge, T. Wang, Y. Ding, et al., Adv. Energy Mater. 12 (2022) 2103916.
[124] W. Yu, Z. Chen, Y. Fu, et al., Adv. Funct. Mater. 33 (2023) 2210855.
[125] Y. Gao, D. Zheng, Q. Li, et al., Adv. Funct. Mater. 32 (2022) 2203206.
[126] Y. Gao, Z. Chen, Y. Zhao, et al., Appl. Catal. B: Environ. 303 (2022) 120879.
[127] Z. Wu, Y. Zhao, W. X, et al., ACS Nano 16 (2022) 18038–18047.
[128] W. Yu, Z. Chen, W. Xiao, et al., Inorg. Chem. Front. 9 (2022) 1847–1855.